

Self-sustained oscillation of a jet impinging upon a Helmholtz resonator

By W. M. JUNGOWSKI† AND G. GRABITZ

Max-Planck-Institut für Strömungsforschung, D-3400 Göttingen, Bunsenstr. 10, FR Germany

(Received 5 January 1984 and in revised form 18 September 1986)

A planar, sonic, underexpanded air jet induced strong and self-sustained flow oscillation. The jet was bounded by two parallel walls extending between the nozzle and the Helmholtz resonator opposite. This oscillation was characterized by large pressure amplitudes in the resonator and periodic displacement of a detached shock wave. The observed phenomena were in some measure similar to those occurring with Hartmann–Sprenger tubes. Based on the experimental results, including Mach–Zehnder interferograms and fluctuating pressure and velocity measurements, the properties of the oscillation have been described and a model for theoretical analysis has been established. Experimental and numerical investigations have made possible a description of the oscillation mechanism, which is of the relaxation type.

1. Introduction

Investigations of free axisymmetric or planar jets and of axisymmetric or planar mixing layers impinging on various obstacles have been described in numerous papers (cf. references in three review papers: Rockwell 1983; Rockwell & Naudascher 1979; Jungowski 1978). The impinging of a gas jet on a cavity – particularly on a Hartmann–Sprenger or resonant tube – has already been under study for a long time. Various potential applications of Hartmann–Sprenger tubes in certain branches of engineering (Smith & Powell 1964; Rozenberg 1969) have stimulated many experiments. Almost all the numerous papers, except two (Przirembel & Fletcher 1978; Przirembel, Fletcher & Wolf 1977), refer to tubes with axisymmetric jets. In a few cases (Smith & Powell 1964; Vrebalovich 1962; Sarohia & Back 1979), the cavity alone had a square or nearly square cross-section. The authors do not know of any results obtained with planar jets, i.e. from a rectangular nozzle and bounded by two parallel walls extending from the nozzle to the cavity. In one paper (Smith & Powell 1964), the early experiments of Hartmann with a Helmholtz resonator are mentioned and repeated.

The oscillation in a cavity was first described by Hartmann. He and his co-workers have published several papers concerning various Hartmann generators. They postulated the *modus operandi* (Hartmann & Trolle 1930) of a simple, basic generator. It was noted that oscillations were excited when the mouth of the cavity was located near the maxima of the total-pressure distribution along the axis of a jet with a cellular structure. Due to the instability of the stagnation interface, the cavity fills and debouches in turn with its natural frequency. Sprenger (1954) was the first investigator to report the thermal aspects of the Hartmann generator. Smith & Powell (1964) analysed and clarified some shortcomings of Hartmann's theory,

† Presently research scientist NOVA/Husky Research Corporation, Calgary, Canada.

largely by identifying the bi-stable condition of the stagnation interface. The position of the interface and stagnation pressure are coupled with the position of the detached shock wave along the jet. This was proven, however, for the axisymmetric jet only. They found that a fully two-dimensional system – enclosing the nozzle, jet flow and cavity between two glass plates – would not oscillate under any combination of circumstances in the absence of an added tripping device. Rozenberg (1969), discussing the results of Hartmann & Trolle (1930) and Boucher & Brun (1958), arrived at the conclusion that a relaxation mechanism is responsible for the oscillation. Sarohia & Back (1979) distinguished three modes of generator operation: the jet instability mode, the jet regurgitant mode and the jet screech mode. The first mode occurred only for a subsonic jet over a wide range of the ratio l/d (l is the spacing between nozzle and resonator and d the exit diameter of a nozzle) and was associated with the formation of large, periodic vortices at the nozzle exit. These toroidal vortices in the jet flow grew in size as they convected downstream and resulted in weak compression waves inside the resonator. The oscillation frequency was found to occur in a narrow range of $St = fd/u$, between 0.3 and 0.4. Sometimes this frequency was superimposed on the fundamental tube resonance frequency. The regurgitant mode is the basic one observed by Hartmann. The screech mode appeared when the cell length of a free jet exceeded spacing l . An almost normal shock oscillated with high frequency and small amplitude in front of the resonator, increasing the temperature inside significantly. The authors supposed that these oscillations were driven by the shear layer emerging from behind this shock and impinging on the resonator inlet.

Many efforts have been devoted to increasing the pressure amplitude and temperature in the resonator. Among them were: optimum selection of a nozzle to resonator cross-sectional area ratio (Rozenberg 1969); insertion of a coaxial rod in the nozzle (Smith & Powell 1964; Brocher, Maresca & Bournay 1970) or central plate extending through a plane nozzle and resonator (Jungowski & Meier 1984); implementation of a tapered (Iwamoto *et al.* 1979), single step (Kawahashi, Bobone & Brocher 1984) or multistep (Brocher & Ardissonne 1983) resonator; and employment of a second resonator (Kawahashi & Suzuki 1974; Brocher & Pinna 1980).

A few attempts were made to develop a theory describing the oscillation mechanism, but none was satisfactory. Mørch (1964), assuming one-dimensional flow along the jet axis between a normal shock and a blunt body as a resonator, derived a linear wave equation and boundary conditions at the shock and at the resonator. As a solution he obtained several resonant frequencies corresponding to various amplification factors. The theory applies, however, to shock oscillation with a small amplitude only. Therefore, it may be adequate for the regurgitant mode with a very short cavity, or possibly also for the screech mode. Thompson (1964) calculated gas oscillation inside a tube resonator by the characteristics method, assuming simple boundary conditions, different for the inflow and outflow phase. Brocher *et al.* (1970), using characteristic equations and introducing some simplifying assumptions, showed that the oscillation in a resonator tends to a 'limit cycle' when certain boundary conditions exist. Kawahashi *et al.* (1974) also applied the characteristics method but included wall friction, heat transfer and interaction on a contact surface. Using some experimental results they introduced more precise boundary conditions for the inflow phase.

Kawahashi & Suzuki (1979) considered the flow between the nozzle and the resonator, as well as an internal flow in the resonator. These flow fields were separated by a hypothetical, massless membrane. The authors applied one-dimensional linear

theory and introduced some experimentally found jet properties. The results showed that the oscillations are self-excited owing to the negative acoustic resistance in certain ranges along the jet. In those unstable ranges, shock vibrations in the axial direction arise, with small amplitude and high frequency.

The present study concerns a planar flow with a Helmholtz resonator instead of the previously investigated axisymmetric flows with quarter-wave resonators. The authors believe that this investigation should make it possible to distinguish more details of the flow patterns than in the axisymmetric case and to show the oscillation mechanism explicitly.

The flow oscillation studied in this paper is one of eight different oscillations identified in the same test facility (Jungowski & Meier 1984) but with different elements facing the jet. The elements were: three Helmholtz resonators, the first one as in the above paper, the second with two perforated and divergent plates joining the nozzle to the resonator, and the third with a plate dividing the nozzle and resonator along the centreplane; a resonator chamber without any neck but with a sharp edge inlet; a quarter-wave resonator; a wedge; and an empty test section with the throttle valve (3), shown in figure 1, facing the jet. Four of these oscillations were previously briefly reported by Jungowski (1982). According to the particular element geometry and the pressure ratio across the nozzle, different flow phenomena were primarily responsible for the occurrence of a self-sustained flow oscillation. These phenomena were instabilities of the detached shock wave, a cellular structure, the shear layer, dead air and a stagnation region, as well as separation at the boundary layer or variation of the flow-rate coefficient.

2. Facility and measurements

2.1. Facility

A cross-section of the experimental apparatus is shown in figure 1(a), with nozzle-neck details shown in figure 1(b). Ambient air was sucked through a rectangular, converging nozzle (1) into a plenum chamber ($H_p = 0.5$ m, $L_p = 0.46$ m, $h = 0.01$ m) in which a Helmholtz resonator (2) was installed ($l = 0.03$ m, $H_r = 0.3$ m, $L_r = 0.187$ m, $H = 0.016$ m, $L = 0.15$ m). The widths of the nozzle, plenum chamber and resonator were equal ($b = 0.1$ m), thus achieving a quasi-two-dimensional flow. The ratio \bar{p} of chamber pressure at the nozzle p_c to ambient pressure p_a was altered by means of a throttle valve (3). A test run could be made by opening a gate valve quickly to connect the plenum chamber to the vacuum reservoir. To diminish the effects of pressure-wave reflections in the plenum chamber, perforated (23%) walls (4) with mineral wool (5) behind them were added. Optical windows (6) enabled flow visualization in the chamber. One window could be replaced by a disk on which a pressure transducer BW and a hot-wire probe SI were mounted. Pressure transducers were also located at six positions on the perforated walls (X, A, B, C, D, E) and in the neck (DI), in the plane of symmetry of the chamber.

2.2. Measurements

The flow was visualized by means of a Mach-Zehnder interferometer, manufactured by Carl Zeiss Ltd. The light source was a spark of 1 μ s duration, which was in an argon chamber. Photographs of the interferograms were taken with a conventional camera and with a high-speed (up to 8000 frames/s) 'Fastax' camera as films.

Time-mean underpressure in the plenum chamber was measured during a test run

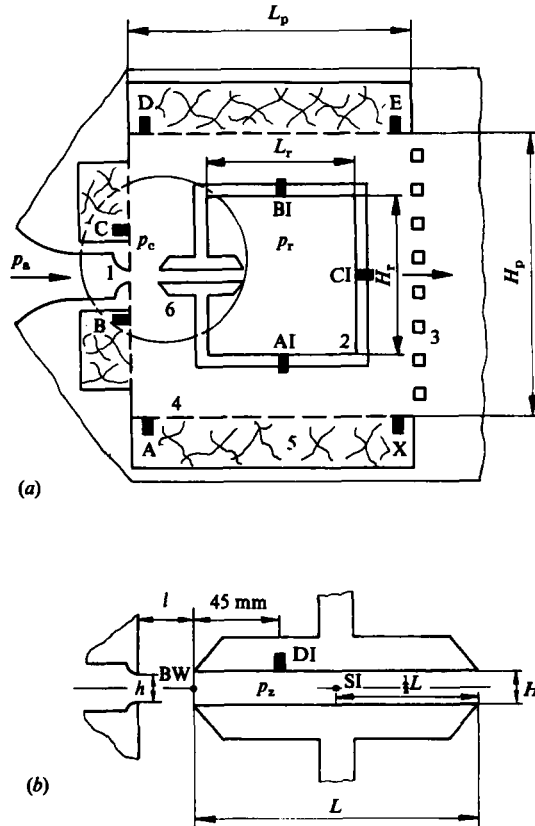


FIGURE 1. (a) Cross-section of experimental apparatus; (b) nozzle-neck details. 1, nozzle; 2, resonator; 3, throttle valve; 4, perforated walls; 5, mineral wool; 6, optical window; X, A, B, C, D, E, BI, CI, DI and BW, pressure transducers; SI, hot-wire probe.

by a digital manometer, fed through a small orifice close to the nozzle lip. This underpressure and atmospheric pressure were processed by an online computer and thus \bar{p} was estimated for each test run.

Miniature, fast-response, piezo-resistive-type transducers (Kulite model XCS-093-15 A or XCS-093-5 D) were used to measure the unsteady surface pressures. These transducers have a linear dynamic range of 100 and 30 kPa respectively and a flat frequency response to 90 kHz. An amplifier with 16 channels was available.

Fluctuating velocity was measured by a tungsten hot-wire ($5\ \mu\text{m}$) constant-temperature anemometer ASM 1 (Stasicki & Meier 1976).

Data from the pressure transducers and from the hot-wire probe were digitized and processed by a PDP 11/34 computer. The analog signals were sampled at various rates according to the system being used. With Converter LPA 11 K, the sampling rate $s.r. = 50/n$ (kHz) depends on the number of probes n . With Transient Recorder Le Croy and Camac-Crate a sampling rate of 200 kHz was adopted. A fast-Fourier-transform (FFT) algorithm was used for calculating the spectra. The frequency constant band in the spectrum corresponding to the higher sampling was 12.207 Hz.

The tests were carried out for $0.4 > \bar{p} > 0.15$, with corresponding Mach numbers at the jet boundary of $1.22 < M < 1.9$.

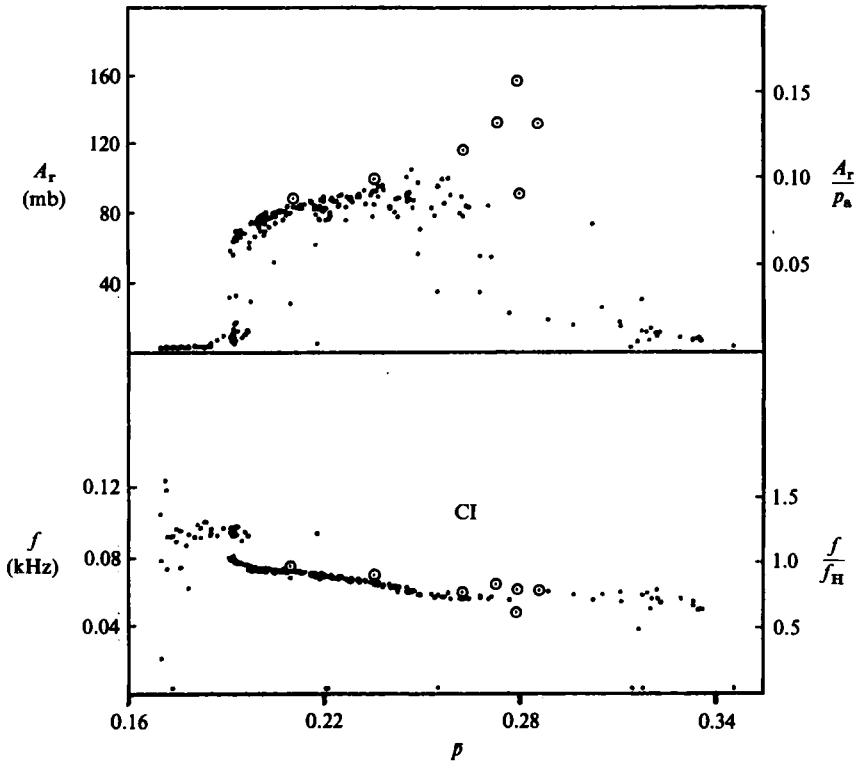


FIGURE 2. Frequency f , (f/f_H) and amplitude A_r , (A_r/p_a) inside the resonator chamber (CI) versus \bar{p} : \cdot , throttle valve opening during the test run; \odot , preset valve position.

3. Experimental results

Figure 2 shows frequency f and pressure amplitude A_r inside the resonator chamber (test point CI) versus \bar{p} . Large amplitudes occur over a pressure range where regular oscillation is observed (see also figure 7). The lower boundary at $\bar{p} = 0.19$ is very distinct and stable, unlike the boundary at a higher $\bar{p} = 0.28$ which is much less distinct and somewhat volatile. The dots result from measurements with continuously increasing \bar{p} controlled by a wider opening of the throttle valve (3) during the test. Data obtained individually with a preset valve position are marked by circles. An increased scatter of the amplitude at the upper boundary of the oscillation could be caused by a too rapidly varying pressure in the test section, thus preventing development of the regular oscillation in that \bar{p} -region in which it appeared sometimes as unstable. The frequency increases with decrease in \bar{p} . This results from a jet cell elongation and thus displacement towards the resonator of the minimum-density area in the cell. We shall discuss this point again with the oscillation mechanism. The maximum pressure amplitude appeared near $\bar{p} \approx 0.28$. The ratio of the measured frequency to the calculated acoustic natural frequency of the Helmholtz resonator $f_H = 75$ Hz varied between 0.65 and 1.08 in the range of the regular oscillation. The natural frequency of the system consisting of the test section and the resonator inside was very close to that of the resonator only.

Typical pressure-time traces (figure 3) and pressure spectra monitored by the transducers BI, CI, E, D, C, B, A, X with the same \bar{p} indicate that the oscillation

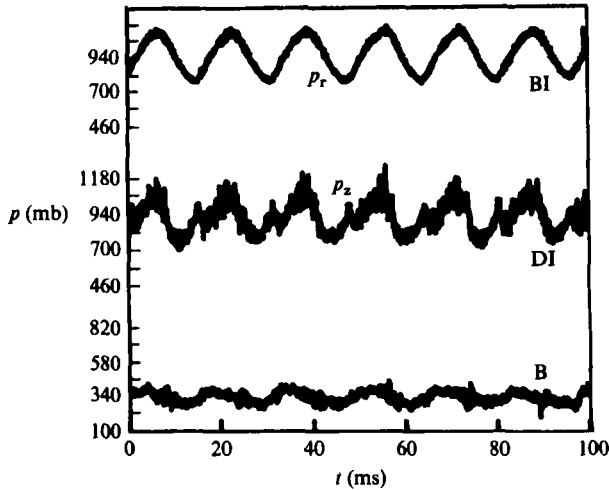


FIGURE 3. Pressure-time traces ($\bar{p} = 0.279$).

is regular and occurs in the whole test section. Pressure amplitudes in the test section, however, are only 16–29% of the amplitude in the resonator. The discrete dominant frequency was equal at all test points and the phase angle measured indicated that pressure signals at the nozzle (B and C) lead the signal in the resonator (CI) by 82° and 110° respectively, but the signals at the horizontal walls of the test section (E, D, A and X) lag by 162° – 168° .

Figure 4 presents a film sequence (1830 frames/s) corresponding to the trace produced by spark discharges (figure 5a) and to the chamber pressure trace (figure 5b). Fifteen frames from numbers 1–29 comprise one period. Figure 5(d, e) show pressure-time traces at the neck lip and at the nozzle respectively. Figure 5(c) contains the time trace of the air velocity u_z in the neck (SI). The letters (a), (b), (c) and (d) in figure 5(a) relate to the interferograms in figure 6 taken at various times. These single interferograms, being of a better quality than movie frames, enabled us to study more details of a flow pattern and allowed us to evaluate density and pressure distributions along the centreplane of the jet (figure 7). Entropy increase, owing to water-vapour condensation indicated in figure 6 by a large gap between fringes somewhat downstream of the nozzle exit, was calculated under the assumption that shock waves in the interferograms (b) and (d) are quasi-stationary. The resulting relative humidity of the air was, in both cases, about 58%. The same entropy increase was used to calculate pressure distributions from interferograms (a) and (c). The decrease in stagnation pressure Δp_{0c} (figure 7b) caused by the condensation was nearly equal to Δp_{0s} which is associated with the shock wave (d). Corresponding instantaneous static pressures measured at the nozzle, at the neck, and in the chamber are shown for comparison in figure 7(b). The arrows indicate flow direction at the neck lip (a, b and d) at the stagnation interface (d). Interferograms in figure 6(a, b) and corresponding curves in figure 7 are associated with the filling phase (figure 5), and therefore the arrows are orientated to the right ($u_z > 0$). The interferogram in figure 6(c) and curve (c) in figure 7 relate to the interphase when $u_z = 0$. Interferogram figure 6(d) and curve (d) in figure 7 belong to the discharge phase when $u_z < 0$. At the beginning of the filling phase, (a), pressure in the chamber is much lower than the

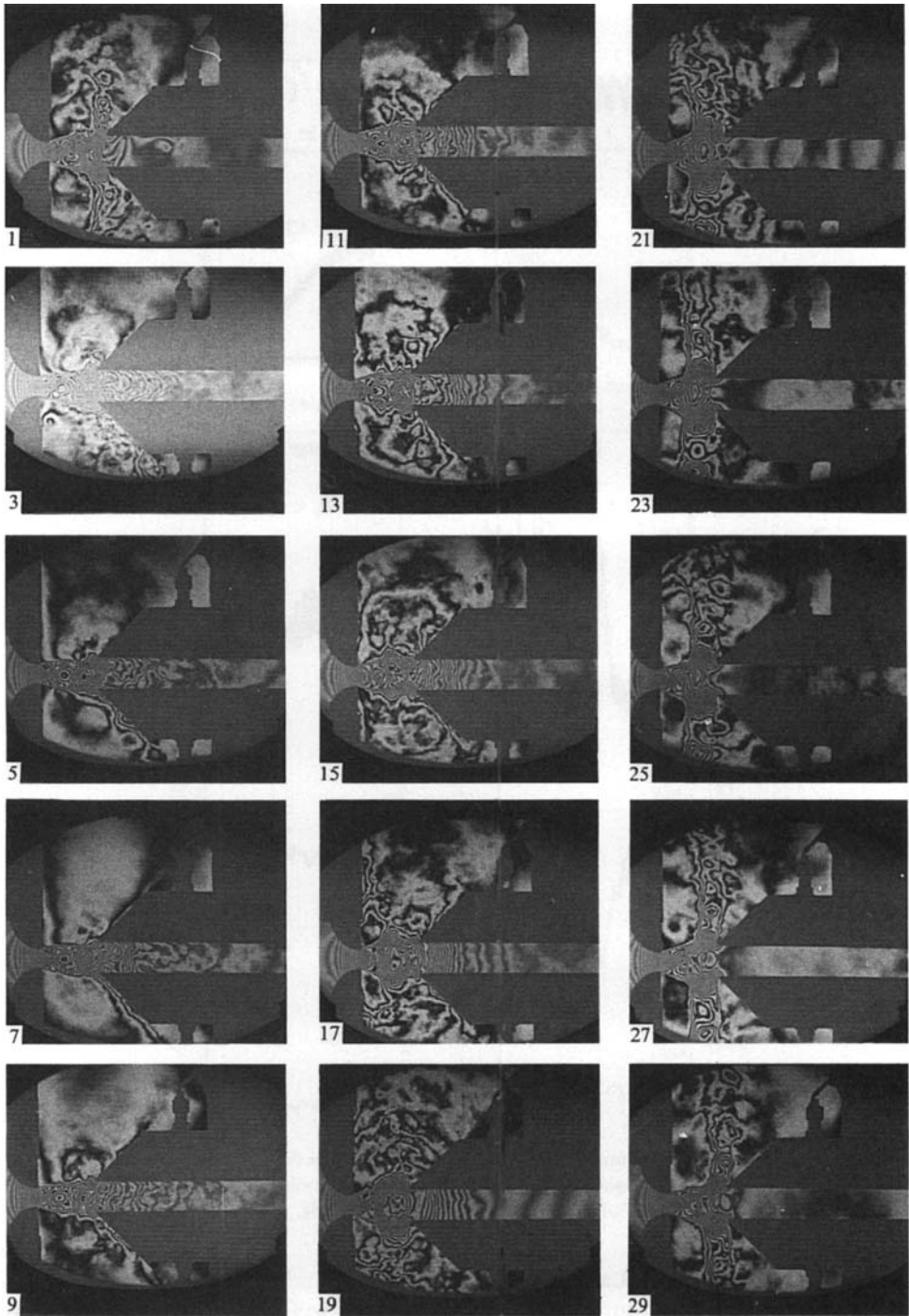


FIGURE 4. One cycle of flow oscillation (interferograms from a film running at 1830 frames/s, $\bar{p} = 0.273$).

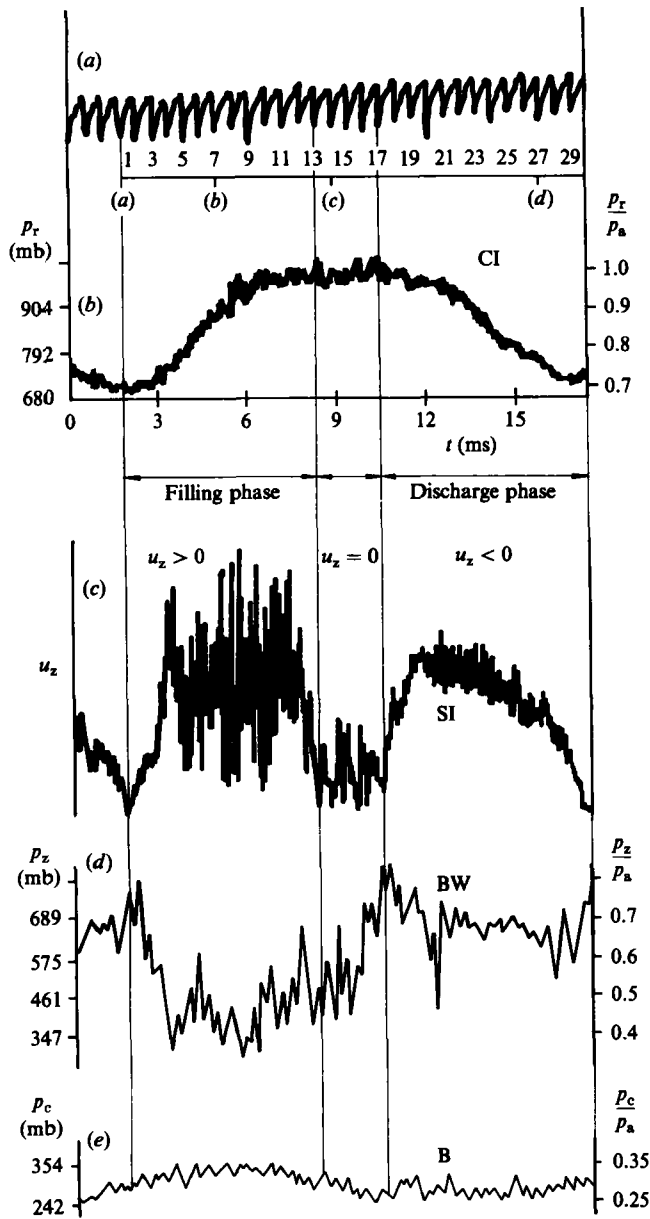


FIGURE 5. Signals monitored simultaneously with the film; $\bar{p} = 0.273$. (a) Light-source signal; (b) pressure signal inside the resonator chamber (CI); (c) flow velocity in the neck (SI); (d) pressure signal at the neck lip (BW); (e) pressure signal at the nozzle (B).

jet stagnation pressure p_0 . Later it is equal to p_0 , (b), and, during the interphase, (c), exceeds p_0 . The static pressures directly measured fit well with those calculated from the density distribution for (a), (b) and (c). Only during the discharge phase (d), are the pressures measured at the neck lip and in the chamber lower than the respective static and stagnation pressures of the jet evaluated from the density distribution. The location of the shock wave, varying within one period and determined from the movie frames, is given with the associated pressure trace in figure 8 (notation

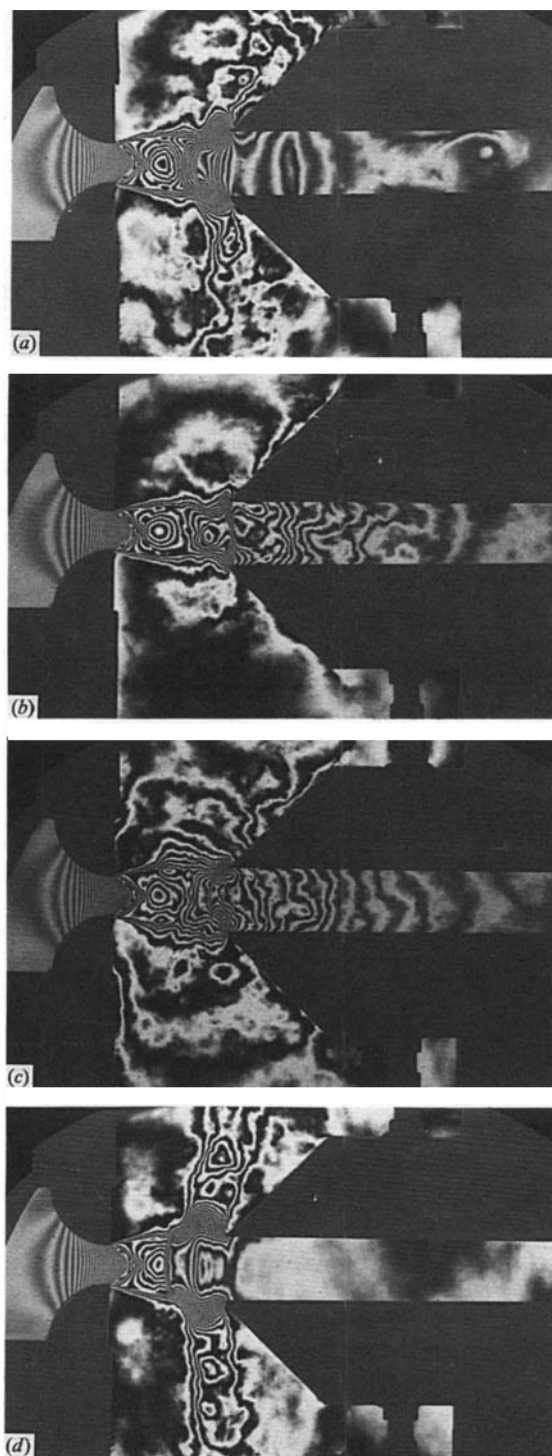


FIGURE 6. Interferograms of the oscillating jet ($\bar{p} = 0.285$).

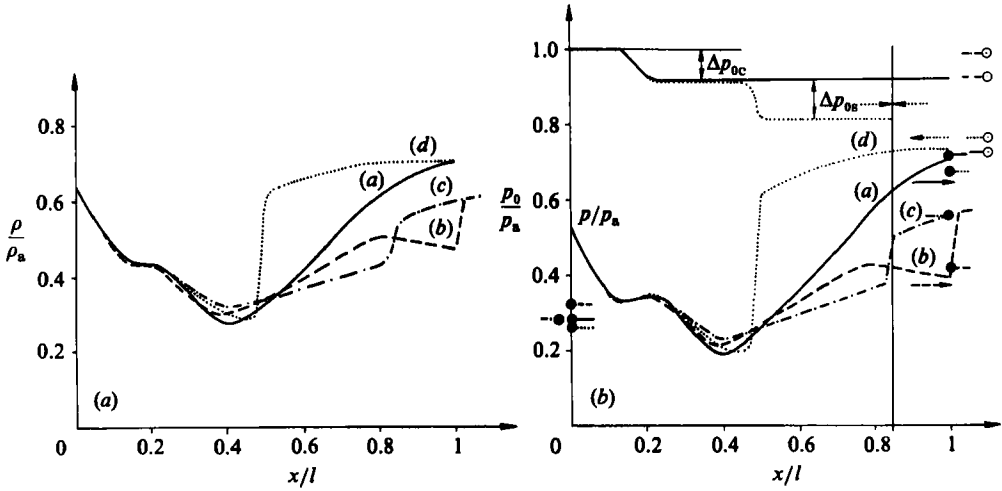


FIGURE 7. Instantaneous distributions along the jet centreline ($\bar{p} = 0.285$), (a) of density and (b) corresponding static and stagnation pressures. Static pressure, measured: ●, at the nozzle ($x/l \neq 0$) and at the neck ($x/l = 1$); ○, in the resonator chamber.

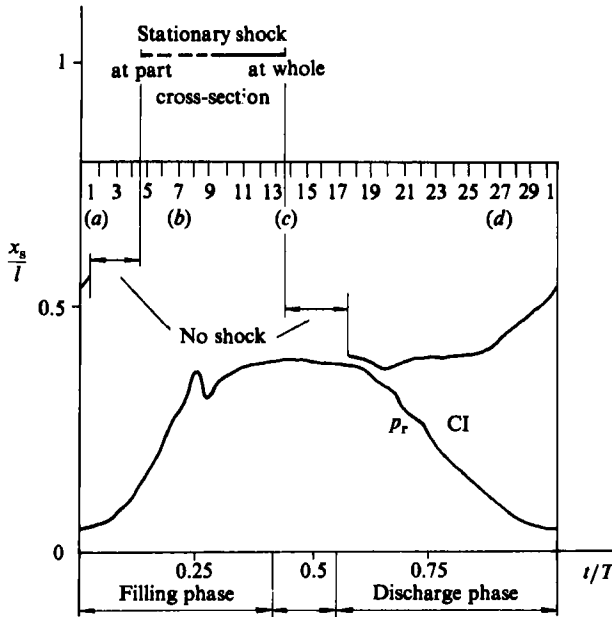


FIGURE 8. Shock-wave location and related pressure signal in the resonator during one period ($\bar{p} = 0.273$, 1-29 denote frame numbers in figure 4, and (a), (b), (c), (d) are from figure 6).

explained in figure 10). At the beginning of the filling phase and before the discharge phase, no shock can be distinguished in the jet structure (frames 3, 15 and 17 in figure 4, and figure 6c). The cells look considerably distorted, perhaps owing to some transverse deformation of the shock front resulting from a rapid propagation along the cell and an interaction with the boundary layer at the sidewalls. The stationary shock at the neck lip re-emerges initially only at some part of the cross-section (frames

5, 7 and 9 in figure 4), extending later across the whole neck (frames 11 and 13 in figure 4).

A study of all the evidence collected in figures 4–8 yielded the following information. In the first frame (figure 4) the jets perpendicular to the centreplane of the nozzle are thin, and the shock wave is heading towards the neck where it disappears for a while (frame 3, figures 6(a) and 8). Minimum chamber pressure (figure 5b), and velocity in the neck equal to zero (figure 5c), indicate the beginning of the filling phase. Displacement of the shock, toward the cell portion in which the Mach number is lower, increases the stagnation pressure and thus generates a sharp pressure peak at the neck lip (figure 5d). This peak in turn develops a pressure wave which appears as a density variation in the neck (frame 1). That density variation is present during the whole filling phase (frames 1–15 and figure 6a, b) and during the beginning of the discharge phase (frames 17, 19 and figure 6c). As the pressure peak is higher than the pressure in the chamber, the air in the neck is accelerated and the velocity increases violently (figure 5c). An expansion wave reflected from the resonator chamber decreases pressure at the neck lip considerably (figure 5d). This process of wave propagation and reflection continues during the filling phase of the chamber (figure 5c, d). Low pressure at the neck lip enables the jet to fill the neck almost without spilling over (frames 5–9 and figure 6b). The tranquility of the region surrounding the jet (frame 7 and figure 6b) corresponds to maximum pressure at the nozzle (figure 5e). The shock wave reappears at the neck lip (figure 8), first partially (frames 5–9) and then over the whole cross-section (frames 11 and 13). Velocity in the neck decreases abruptly (figure 5c), indicating the end of the filling phase. When the pressure in the chamber exceeds the stagnation pressure of the jet, the shock wave moves upstream (figure 8) and the cellular structure becomes irregular (frames 15, 17 and figure 6c). This is followed by some fluctuation in velocity and by a pressure increase in the neck (figure 5d). The pressure then decreases, owing primarily to an increase in velocity (frames 17, 19 and figure 5c) and to a decrease in the chamber pressure (frames 19–29, figures 6d, 5b). On frame 19 the shock reappears a little upstream of minimum density. Velocity in the neck decreases gradually (frames 21–29 and figure 5c). During the discharge phase, the shock moves slowly downstream (figure 8) towards minimum density and thus the cycle may start again.

When compared to the mathematical model described in §4, it should be emphasized that density gradients in the neck appeared along only about one third of its length (figures 4 and 6). The most significant density variation occurred close to the neck lip. Corresponding pressure-time traces obtained with the transducers BW and DI (figures 1, 5d and 3) differ considerably. Most probably, density and pressure variations close to the neck lip depend substantially upon a locally fluctuating flow pattern, resulting from pressure-wave reflections at the neck lip. During the filling phase, in particular, strong pressure and velocity oscillation (≈ 1.1 kHz) was excited in the neck (figure 5c, d).

It is possible that the shock wave at the lip (figure 8) was also involved in that oscillation. The film speed (1830 frames/s) was, however, too low to expose a shock displacement with high frequency and small amplitude. All the phenomena mentioned above were omitted in the theoretical considerations.

Normalized cell length (L_c/h , L_c/l) and position of minimum density (L_m/h , L_m/l) with corresponding maximum Mach number are shown versus \bar{p} in figure 9. They were evaluated from the interferograms obtained with the empty plenum chamber, i.e. without the resonator. We can observe that the oscillation with a large pressure

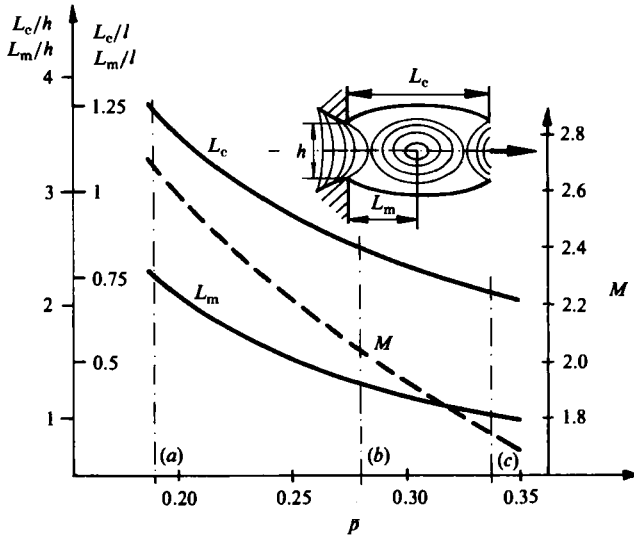


FIGURE 9. Normalized cell length L_c and position of minimum density L_m with a corresponding Mach number M .

amplitude (a - b range of \bar{p} in figure 9, see also figure 2) occurs when the spacing between the nozzle and the neck ($l/h = 3$) is close to the cell length of a free jet ($L_c/h = 3.75$ - 2.5 , $L_c/l = 1.25$ - 0.83). Within the range (b - c) the pressure amplitude was small and outside the range (a - c) the oscillation did not occur at all.

The range of oscillation (a - b) given above is slightly different from that determined by Hartmann & Trolle (1930). Experimenting with axisymmetric jets they kept the pressure ratio \bar{p} constant but varied the spacing l . The ranges established were: $L_c/l = 1.1$ - 0.72 with $\bar{p} = 0.286$ and $L_c/l = 1.077$ - 0.73 with $\bar{p} = 0.253$. A different neck to nozzle area ratio (Hartmann & Trolle 1.015 against our 1.6) could also contribute to a discrepancy between the compared results.

4. Theory

The aim of a mathematical flow model, presented here, is to study the basic, low-frequency oscillation by means of a numerical computation. The simplifying assumptions made the equations simple and easy to solve, but the influence of the most important parameters was still retained.

As basic time-dependent differential equations we use the unsteady Bernoulli equation for the flow in the neck of the resonator and the equation of conservation of mass in the resonator chamber. The flow field between the shock wave and the resonator neck is considered as quasi-steady, i.e. the time-dependent flow variables fulfil the steady conservation equations in this area. This simplification is acceptable because the flow region between the shock wave and the resonator is small when compared to the length L of the neck, which means that the space integral over the acceleration can be neglected in this region.

We distinguish between the three different types of flow fields which are shown in figure 10. First, we consider the attached flow field during the filling phase (figure 10*a*). The variables p , ρ , u and t denote pressure, density, velocity and time,

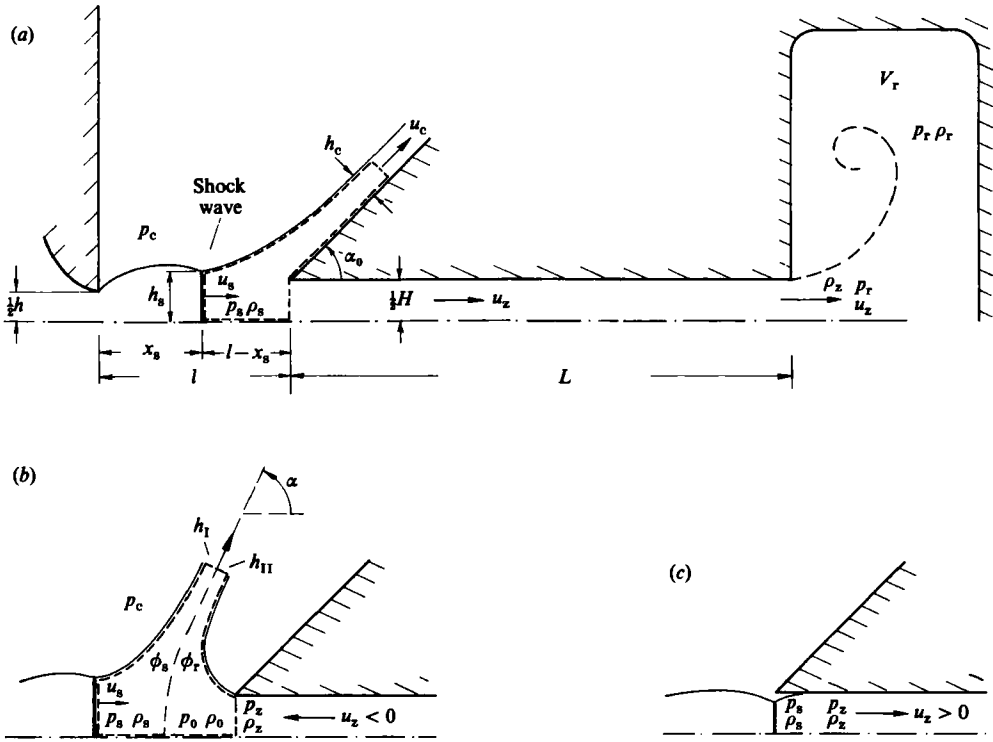


FIGURE 10. Symbols and schematic diagrams of three possible flow fields in front of the resonator. (a) Attached flow field during filling phase; (b) discharge phase; (c) the whole jet flows into the resonator.

respectively. The subscripts r and z correspond to the resonator chamber and to the resonator neck; γ is the ratio of specific heats. The velocity in the neck is $u_z > 0$ and the Bernoulli equation of the form

$$L \frac{du_z}{dt} = \frac{\gamma}{\gamma - 1} \frac{1}{\rho_z} (p_z - p_r) \quad (1)$$

can be applied when viscosity and heat conduction are neglected and the flow variables in the neck are assumed to be functions of time only. As we will show later, (7), the entropy in the neck is different from that in the resonator chamber during the filling phase. Therefore, at the same pressure, the density at the exit of the neck and in the inner chamber must be different. Thus, the density in the neck ρ_z , being dependent on time only, also prevails at the exit of the neck (figure 10a). The experiments exposed a complicated flow pattern in the neck, discussed in the previous section. It seems, however, that the variation of flow along the neck associated with high-frequency oscillations has an insignificant influence on the basic oscillation.

The following unsteady frequency describes the conservation of mass in the resonator chamber:

$$V_r \frac{d\rho_r}{dt} = u_z \rho_z F_z, \quad (2)$$

where V_r is the volume of the chamber and F_z the cross-sectional area of the neck.

Quasi-steady conservation equations of mass and momentum in the α_0 direction, according to the control surface in figure 10(a), are

$$\rho_s u_s h_s - \rho_c u_c h_c - \frac{1}{2} \rho_z u_z H = 0, \quad (3)$$

$$\begin{aligned} (\rho_s u_s^2 + p_s - p_c) h_s \cos \alpha_0 - \rho_c u_c^2 h_c - \frac{1}{2} (\rho_z u_z^2 + p_z - p_c) H \cos \alpha_0 \\ + \left(\frac{p_s + p_z}{2} - p_c \right) (l - x_s) \sin \alpha_0 = 0. \end{aligned} \quad (4)$$

The subscripts s and c correspond to the variables behind the shock wave and the variables of the lateral jet in the plenum chamber. In our one-dimensional approximation, flow variables depend on the cross-section of the jet and are functions of time only. The pressure integral along the axis is approximated by the trapezoidal rule.

In our considerations, the pressure distribution between the nozzle and the shock wave resembles the distribution along the axis of a planar and steady jet. We make use of the minimum pressure p_m , its position L_m , and the position L_c of a maximum pressure obtained by experiment with a steady jet when there was no resonator in the plenum chamber (figure 9). In terms of these values, the pressure in front of the shock wave is given by a parabolic approximation:

$$p_1(x) = \begin{cases} (p^* - p_m) \left(\frac{x - L_m}{L_m} \right)^2 + p_m & \text{for } x \leq L_c, \\ (p^* - p_m) \left(\frac{2L_c - x - L_m}{L_m} \right)^2 + p_m & \text{for } x > L_c, \end{cases} \quad (5)$$

and is plotted in figure 11 (p^* is the critical pressure). The cross-section of the jet and the remaining flow variables are obtained by one-dimensional theory. Therefore, the flow variables behind the shock are given as functions of the distance x_s between the nozzle and the quasi-stationary shock. A different position of the shock wave results in a different shock strength, and this means a different stagnation pressure and stagnation density behind the shock. Stagnation parameters (p_a, ρ_a) upstream and the flow variables (p_s, ρ_s) behind the shock wave are combined in (6),

$$\frac{p_s}{\rho_s^\gamma} = \frac{p_a}{\rho_a^\gamma} \phi_s, \quad (6)$$

where the function $\phi_s(t)$ is an additional variable given by the shock conditions and showing the entropy increase. For the resonator chamber the relationship may be written similarly as

$$\frac{p_r}{\rho_r^\gamma} = \frac{p_a}{\rho_a^\gamma} \phi_r. \quad (7)$$

The gas filling the resonator chamber suffers varying irreversible processes. Entropy increases owing to the shock wave and friction along the neck, and owing to the dissipation of kinetic energy inside the chamber. An accurate computation of that entropy increase during the filling phase seems to be impossible for several reasons. Therefore, the processes of compression and expansion in the chamber are assumed to be isentropic but occurring at an increased entropy level represented by the parameter ϕ_r ; that means we suppose that this parameter depends on the weighted mean entropy increase. Instead of the density we introduce ϕ into our equations.

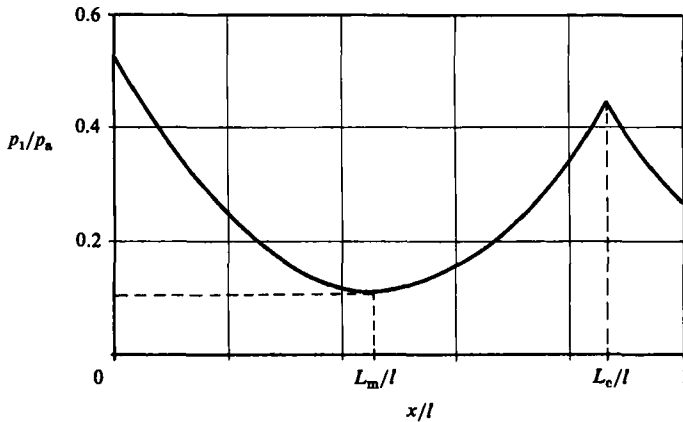


FIGURE 11. Pressure in front of the shock wave (model of the undisturbed free jet with dimensionless plenum pressure $\bar{p} = 0.27$).

With the dimensionless time $\tau = tc^*/h$ (c^* is the critical velocity of sound) the differential equations (1) and (2) then become

$$\frac{d}{d\tau} \left(\frac{u_z}{c^*} \right) = \left\{ \left[1 - \left(\frac{u_z}{c^*} \right)^2 \frac{\gamma - 1}{\gamma + 1} \right]^{\gamma/(\gamma - 1)} - \left(\frac{p_r}{p_a} \right) \phi_s^{1/(\gamma - 1)} \right\} \times \left[1 - \left(\frac{u_z}{c^*} \right)^2 \frac{\gamma - 1}{\gamma + 1} \right]^{-1/(\gamma - 1)} \frac{\gamma + 1}{2(\gamma - 1)} \frac{h}{L}, \quad (8)$$

$$\frac{d}{d\tau} \left(\frac{p_r}{p_a} \right) = \gamma K \left(\frac{p_r}{p_a} \right)^{(\gamma - 1)/\gamma} \frac{u_z}{c^*} \left[1 - \left(\frac{u_z}{c^*} \right)^2 \frac{\gamma - 1}{\gamma + 1} \right]^{1/(\gamma - 1)} \phi_r^{1/\gamma} \phi_s^{-1/(\gamma - 1)}. \quad (9)$$

The constant K is given in terms of the geometrical quantities as $K = F_z h / V_r$.

In order to obtain ϕ_s from the shock relations with the help of (5), the position x_s of the shock wave must be known. We get x_s from the conservation equations of mass and momentum, (3), (4).

Thus, for the given initial values, the system of ordinary differential equations (8) and (9) which is valid for $u_z > 0$, can be solved numerically for the pressure p_r in the resonator and the velocity u_z in the neck. Input parameters are the geometrical quantities, the quantity ϕ_r and the pressure p_c in the plenum chamber, which also determines the pressure distribution along the undisturbed free jet (figure 9, equation (5) and figure 11).

A special case occurs (figure 10c) when the whole jet flows into the resonator. Then the shock wave remains at the lip of the neck so that the pressure p_z during this phase is constant in time and, as will be shown later (figure 12), $p_z > p_r$. The flow in the neck is subsonic and thus p_z should be equal to p_r at the outlet of the neck. In a real compressible flow these boundary conditions imposed at the two ends of the neck are responsible for the generation of the high-frequency oscillation. This complicated unsteady process cannot be described by the simple equation (1). On the other hand, this unsteady flow can be approximated by a steady, time-average flow occurring until $p_z = p_r$. Therefore, when the shock is situated at the lip of the neck we shall assume the flow in the neck to be steady and resulting from an isentropic compression of the gas behind the shock.

During the discharge phase ($u_z < 0$), the gas in the neck of the resonator has the

same entropy level as the gas in the resonator chamber (see figure 10*b*). Thus the Bernoulli equation applied to the resonator chamber and the neck exit yields

$$L \frac{du_z}{dt} = \frac{u_z^2}{2} + \frac{\gamma}{\gamma-1} \frac{p_z}{\rho_z} - \frac{\gamma}{\gamma-1} \frac{p_r}{\rho_r} \quad (10)$$

or

$$L \frac{du_z}{dt} = \frac{\gamma}{\gamma-1} \left(\frac{p_0}{\rho_0} - \frac{p_r}{\rho_r} \right), \quad (11)$$

where p_0, ρ_0 are stagnation pressure and density at the stagnation point shown in figure 10*(b)*. The stagnation values behind the shock depend on the stagnation values in front of the shock as

$$\frac{p_0}{\rho_0^\gamma} = \frac{p_a}{\rho_a^\gamma} \phi_r. \quad (12)$$

The density in the resonator ρ_r can be eliminated using (7), and p_0 by the upstream condition

$$\frac{p_0}{p_a} = \phi_s^{-1/(\gamma-1)}. \quad (13)$$

With the dimensionless time $\tau = tc^*/h$, the differential equation (11) becomes

$$\frac{d}{d\tau} \left(\frac{u_z}{c^*} \right) = \left[\phi_s^{-1/\gamma} - \left(\frac{p_r}{p_a} \right)^{(\gamma-1)/\gamma} \right] \frac{\gamma+1}{2(\gamma-1)} \frac{h}{L} \phi_r^{1/\gamma}. \quad (14)$$

The equation of mass conservation in the resonator, (2), for the discharge phase ($u_z < 0$) transforms to

$$\frac{d}{d\tau} \left(\frac{p_r}{p_a} \right) = \gamma K \left(\frac{p_r}{p_a} \right)^{(\gamma-1)/\gamma} \frac{u_z}{c^*} \left(\frac{p_z}{p_a} \right)^{1/\gamma} \quad (15)$$

because of

$$\frac{p_z}{\rho_z^\gamma} = \frac{p_a}{\rho_a^\gamma} \phi_r. \quad (16)$$

With (12) and (13) and

$$\frac{u_z^2}{2} + \frac{\gamma}{\gamma-1} \frac{p_z}{\rho_z} = \frac{\gamma}{\gamma-1} \frac{p_0}{\rho_0}, \quad (17)$$

one derives

$$\frac{d}{d\tau} \left(\frac{p_r}{p_a} \right) = \gamma K \left(\frac{p_r}{p_a} \right)^{(\gamma-1)/\gamma} \frac{u_z}{c^*} \left[\phi_s^{-1/\gamma} - \left(\frac{u_z}{c^*} \right)^2 \frac{\gamma-1}{\gamma+1} \phi_r^{-1/\gamma} \right]^{1/(\gamma-1)}. \quad (18)$$

In the detached flow field the lateral jets consist of two parts which are of different entropy levels (see figure 10*b*):

$$h_{\text{I}} = \frac{1}{2} h \frac{c^* \rho^*}{u_{\text{I}} \rho_{\text{I}}}, \quad (19)$$

$$h_{\text{II}} = -\frac{1}{2} H \frac{u_z \rho_z}{u_{\text{II}} \rho_{\text{II}}}. \quad (20)$$

The velocities are

$$u_{\text{I}} = \left(\frac{\gamma+1}{\gamma-1} \left[1 - \left(\frac{p_c}{p_a} \right)^{(\gamma-1)/\gamma} \right] \phi_s^{1/\gamma} \right)^{\frac{1}{2}}, \quad (21)$$

$$u_{\text{II}} = \left(\frac{\gamma+1}{\gamma-1} \left[\phi_s^{-1/\gamma} - \left(\frac{p_c}{p_a} \right)^{(\gamma-1)/\gamma} \right] \phi_r^{1/\gamma} \right)^{\frac{1}{2}}, \quad (22)$$

and the densities are

$$\rho_{\text{I}} = \left(\frac{p_{\text{c}}}{p_{\text{a}}} \right)^{1/\gamma} \phi_{\text{s}}^{-1/\gamma}, \quad (23)$$

$$\rho_{\text{II}} = \left(\frac{p_{\text{c}}}{p_{\text{a}}} \right)^{1/\gamma} \phi_{\text{r}}^{-1/\gamma}. \quad (24)$$

Now, in the case of a detached flow with a stagnation point on the axis, we use the quasi-steady equations of conservation of momentum in the axial direction and in the direction perpendicular to the axis. The angle α is an additional variable:

$$h_{\text{s}}(\rho_{\text{s}} u_{\text{s}}^2 + p_{\text{s}} - p_{\text{c}}) - \frac{1}{2}(\rho_{\text{z}} u_{\text{z}}^2 + p_{\text{z}} - p_{\text{c}}) H - (\rho_{\text{I}} u_{\text{I}}^2 h_{\text{I}} + \rho_{\text{II}} u_{\text{II}}^2 h_{\text{II}}) \cos \alpha = 0, \quad (25)$$

$$(\rho_{\text{I}} u_{\text{I}}^2 h_{\text{I}} + \rho_{\text{II}} u_{\text{II}}^2 h_{\text{II}}) \sin \alpha - (l - x_{\text{s}}) \left(\frac{p_{\text{s}} + 4p_{\text{o}} + p_{\text{z}}}{6} - p_{\text{c}} \right) = 0. \quad (26)$$

The pressure integral along the axis is approximated by the Simpson formula and the stagnation point is assumed to be in the middle between the shock wave and the lip of the resonator neck.

With the help of (25) and (26) the differential equations which are valid for $u_{\text{z}} < 0$ can be solved numerically too.

Our simple theory gives, at $u_{\text{z}} = 0$, an unsteadiness in the pressure in the neck of the resonator, because of the sudden change of the entropy level in the neck. And thus a jump from the attached to detached flow field occurs, and vice versa.

5. Numerical results

The simple theoretical model, given in §4, describes the very complicated flow field with only a few variables. In particular, the flow situations in the resonator chamber as well as those in the resonator neck are represented by only one set of time-dependent flow variables. The time-dependent position of the shock wave x_{s} (for notation see figure 10*a*) is approximately determined from the quasi-steady conservation equations in the integral form. Such a model is obviously not able to show details of the flow field. The question is whether our theoretical model shows self-sustained oscillations similar to those obtained in the experiments, and thus whether an insight into the oscillation mechanism is given.

Input parameters are, beside the geometrical quantities, the dimensionless pressure in the plenum chamber $\bar{p} = p_{\text{c}}/p_{\text{a}}$ (figures 1, 10*a*) and the parameter ϕ_{r} (see equation (7)). The pressure in the plenum chamber also determines the pressure distribution along the undisturbed free jet (equation (5), figure 11). In this model of the free jet in front of the shock wave we make use of the minimum pressure, its position and the position of the maximum pressure obtained from an experiment with a steady jet when there was no resonator in the plenum chamber (figure 9). The input parameter ϕ_{r} (equation (7)), which depends on the mean entropy increase in the resonator chamber, is unknown. We shall show that the ϕ_{r} value introduced into the computation is realistic and physically justified.

The ordinary-differential-equation system was solved using the Runge–Kutta method. The geometrical input parameters corresponding to the experiments were: $K = F_{\text{z}} h / V_{\text{r}} = 1.6/506$, $L/h = 15$, $l/h = 3$ and $H/h = 1.6$.

The numerical results given in figure 12 are for a pressure in the plenum chamber of $p_{\text{c}}/p_{\text{a}} = \bar{p} = 0.24$ and the parameter $\phi_{\text{r}} = 1.12$. The initial condition for the pressure in the resonator ($p_{\text{r}} = p_{\text{c}}$) means that the gas is flowing through the neck of the resonator at the maximum possible velocity; i.e. we start with a flow field

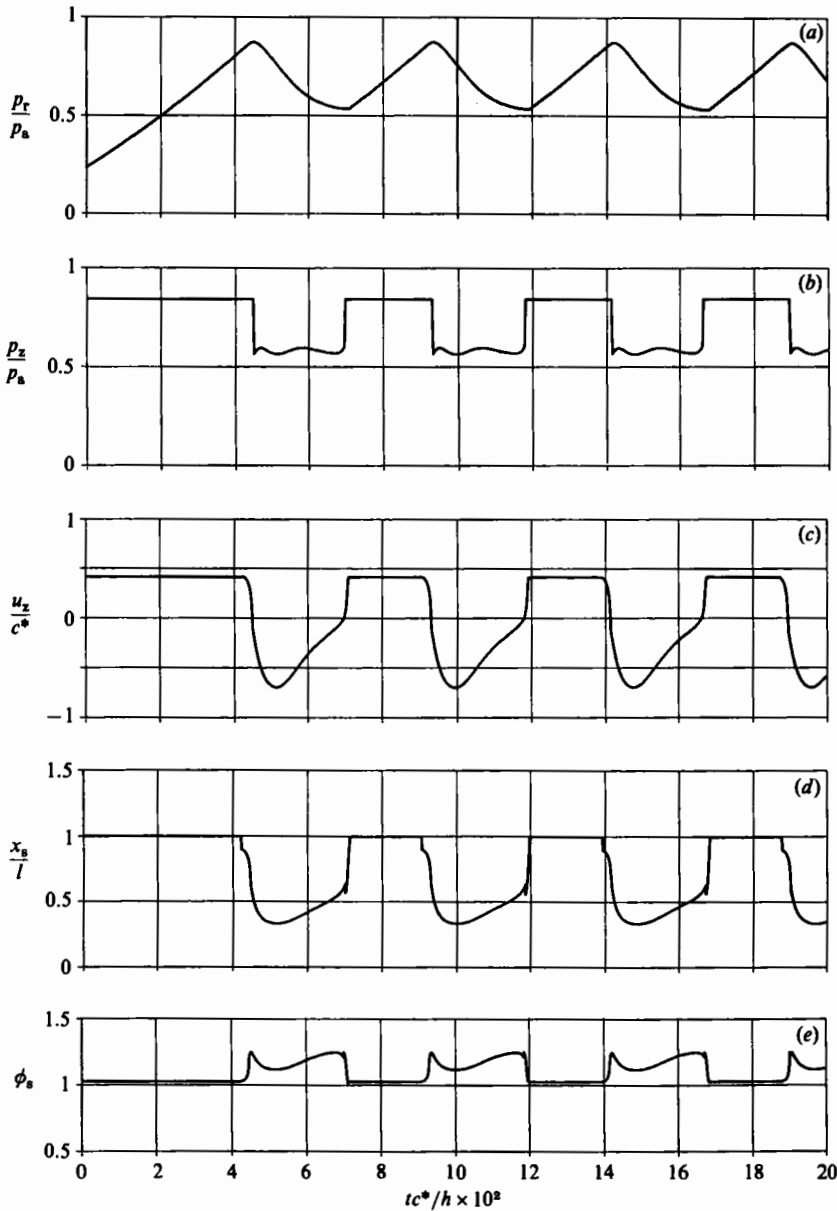


FIGURE 12. Variation in time of (a) pressure p_r in the resonator chamber, (b) pressure p_z in the neck, (c) velocity u_z in the neck, (d) position x_s of the shock wave and (e) ϕ_s (equation 6) for $\phi_r = 1.12$ and $\bar{p} = 0.24$.

corresponding to the shock wave position at the lip of the resonator neck (figure 10c). When the pressure p_r in the resonator reaches the level of the pressure p_z in the neck, the shock wave will move upstream and the flow field will be formed as shown in figure 10(a). With increasing pressure p_r in the resonator, the velocity in the neck decreases and eventually the flow turns around. After the subsequent discharge phase, the flow field is as shown in figure 10(b), and the pressure p_r becomes low enough to accelerate the gas to the maximum velocity again. Thus a regular self-sustained oscillation,

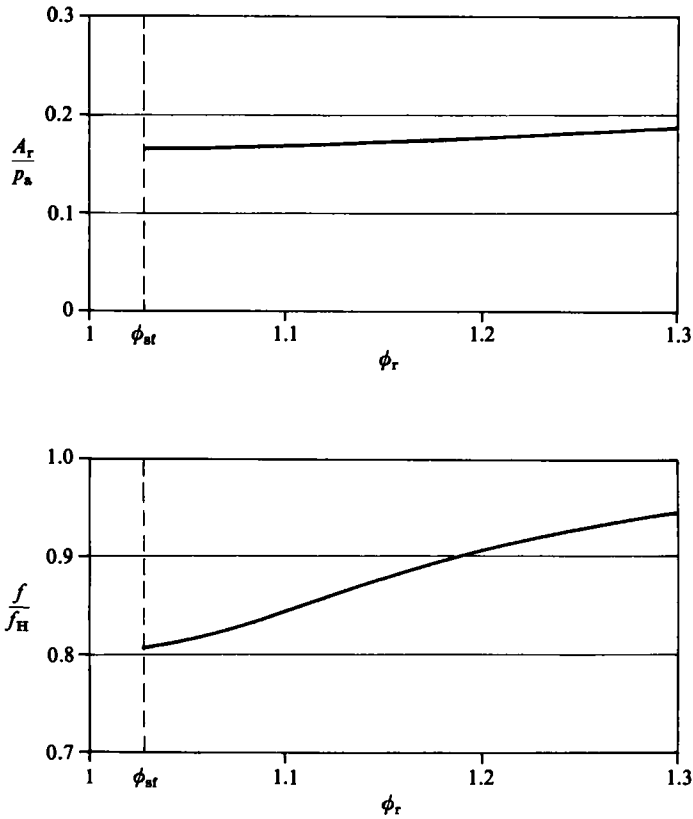


FIGURE 13. Non-dimensional amplitude A_r/p_a and frequency f/f_H (f_H is the Helmholtz frequency) of the oscillation versus ϕ_r ($\bar{p} = 0.24$).

similar to that obtained in the experiments, occurred. The computed frequency $f \approx 65$ Hz is the same as the corresponding experimental value (see figure 2) because of the special choice of the parameter ϕ_r . The predicted non-dimensional amplitude of the pressure p_r is 0.17 against the experimental one of 0.1. The computed non-dimensional amplitude of the pressure p_z is 0.14 and it fits well to the experimental amplitudes 0.15, 0.14 and 0.15 obtained with the three different levels of \bar{p} of 0.273 (figure 5*d*), 0.279 (figure 3) and 0.285 (figure 7) respectively. A qualitative agreement between the theoretical and experimental velocity-time traces (figure 5*c*) can be observed, if the high-frequency oscillation in the neck during the filling phase is also neglected and the velocity during the discharge phase is plotted as a negative one. A comparison of curve (*d*) in figure 12 with the corresponding curve in figure 8 shows a small discrepancy between the extreme positions of the shock wave calculated from the theory ($1 \geq x_s/l \geq 0.30$) and measured in the experiment ($1 \geq x_s/l \geq 0.38$). It should be stressed, however, that the experimental shock position was obtained with a different \bar{p} (0.285) than the numerical one (0.24). The time-trace of ϕ_s (figure 12, curve *e*) shows a strong dependence on the position of the shock wave.

The influence of the parameter ϕ_r on the non-dimensional amplitude and frequency is shown in figure 13 ($\bar{p} = 0.24$). The lower limit $\phi_{st} = 1.033$ means that ϕ_r resulted from a mean increase in entropy only at the shock wave during the filling phase.

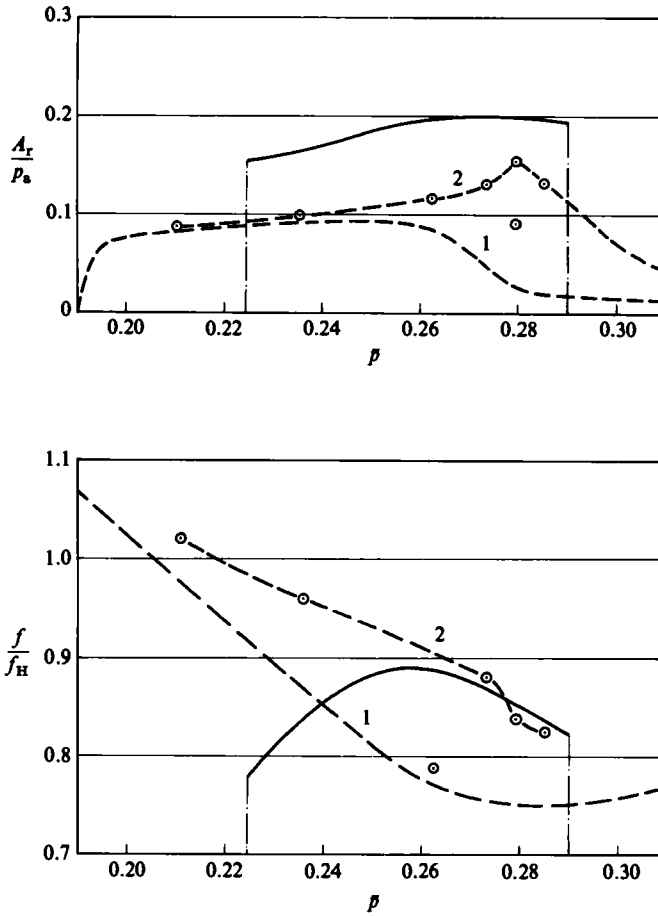


FIGURE 14. Non-dimensional amplitude A_r/p_a and frequency f/f_H (f_H is the Helmholtz frequency) of the oscillation versus \bar{p} ($\phi_r = 1.12$). Dashed lines, experimental data from figure 2; 1, valve opened continuously; 2, preset valve position.

Over a wide range of ϕ_r (from 1.033 to 1.3) the amplitude differs by 13.5% and the frequency by 17% compared to the quantities resulting from ϕ_{sr} . A very crude estimation of ϕ_k , related to the entropy increase caused by the inlet and friction losses of the neck and by a dissipation of kinetic energy in the resonator chamber, follows. The heat generated by these processes can be expressed in the following form:

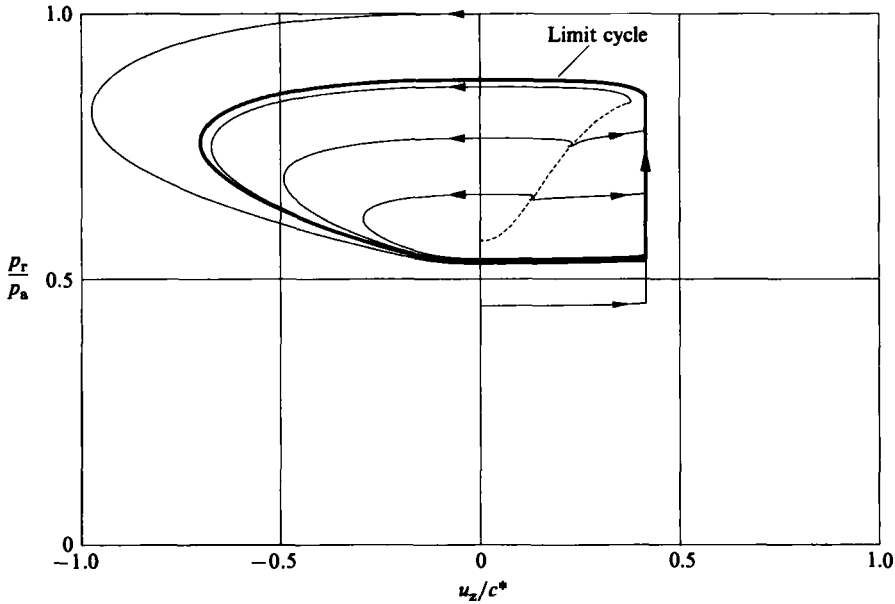
$$\Delta q = \left(\xi + \lambda \frac{L}{H} + 1 \right) \frac{u_z^2}{2}, \tag{27}$$

where ξ and λ denote inlet and friction coefficients respectively. The corresponding entropy increase will be

$$\Delta S = \frac{\Delta q}{T_{av}}, \tag{28}$$

with T_{av} being the average of the varying temperatures in the neck and resonator chamber. ϕ_k can be then obtained from

$$\phi_k = \exp \frac{\Delta S}{c_v} \tag{29}$$


 FIGURE 15. (u_z, p_r) -plane for $\phi_r = 1.12$ and $\bar{p} = 0.24$.

or, after transformation of (29), from

$$\phi_k = \exp \frac{\gamma R(\xi + \lambda(L/H) + 1)}{(\gamma + 1)c_v} \frac{T_a}{T_{av}} \left(\frac{u_z}{c^*} \right)^2. \quad (30)$$

Assuming $\xi = 0.2$, $\lambda = 0.025$, $T_{av} = T_a$ (T_a denotes the jet stagnation temperature) and taking (from figure 12) $u_z/c^* = 0.425$ we calculate $\phi_k = 1.062$ and then $\phi_r = \phi_{sf} \phi_k \approx 1.1$

This value of ϕ_r results in a frequency about 1% lower (figure 13) than the value of $\phi_r = 1.12$ which was used in the example with $\bar{p} = 0.24$ (figure 12) and yielded the same frequency as the experiment. It must be admitted that in the above assessment T_{av} was selected only on the basis of the following general discussion.

In the Hartmann-Sprenger generator with a quarter-wave resonator the time-mean temperature of the indigenous gas results from a thermal balance between the heat generated by the shock wave and friction in the resonator on one side, and heat transferred through the wall and contact surface on the other. When the thermal capacity of the resonator is small this temperature will be established very rapidly.

In the facility under consideration, the resonator chamber had metal walls of 25 mm thickness resulting in a considerable thermal capacity. Moreover, the resonator chamber was surrounded by the flow in the plenum chamber. The temperature in the neck resulting from the flow velocity was $\approx 0.95 T_a$. Isentropic compression and a pressure ratio in the chamber of $p_{r \min}/p_{r \max} \approx 0.8$ would result in the temperature ratio of $T_{r \min}/T_{r \max} \approx 0.94$. In these circumstances, it is very doubtful that during a test run (typically 30 s) T_{av} could exceed T_a .

The parameter $\phi_r = 1.12$ seems to be a good approximation for the whole range of pressures in the plenum chamber considered, because there are only slight differences in the values of ϕ_{sf} , and the additional entropy increase which depends on the velocity in the neck of the resonator during the filling phase is also nearly the same for this pressure range.

In figure 14, results with varying pressure in the plenum chamber and with $\phi_r = 1.12$ are given. Outside the pressure region $0.225 < \bar{p} < 0.29$ the self-sustained oscillation did not occur. To enable a direct comparison with the experiment, the data from figure 2 were replotted as dashed lines in figure 14. The best coincidence of frequency, amplitude and boundary of the oscillation is apparent for high values of \bar{p} . There is a considerable discrepancy in the frequency trend and in the lowest value of \bar{p} where oscillation takes place.

The influence of different initial conditions can be seen in the (u_z, p_r) -plane (figure 15). The limit cycle, which corresponds to the self-sustained oscillation, is reached by outer and inner phase curves. The dashed line is the origin of phase curves leading in different directions. Our experimental results provide no information about the inner phase curves.

6. Mechanism of the oscillation

The experimental correlation of all the phenomena and the theoretical study led to the following description of the oscillation.

During almost the whole filling phase, the shock wave remains attached to the neck lip and thus is close to the end of the first jet cell. As figure 9 indicates, regular oscillation occurred when the ratio of the cell length L_c to the spacing l between the nozzle and neck lip was between 0.82 and 1.25. The Mach number at the centreline around the cell end is relatively low and therefore stagnation pressure downstream of the shock high. When pressure p_r in the resonator chamber exceeds pressure p_z in the neck, resulting from the shock position at the neck lip, the flow velocity u_z in the neck is tending to zero and the shock will be detached and displaced upstream, as in front of a blunt body or the inlet of a choked diffuser. With $L_c < 1$, the shock propagation along the second cell may further increase p_r due to the growing of p_0 , until it is swept into the first cell. There, it cannot stop, because stagnation pressure becomes less than p_r and is decreasing with the shock propagation upstream owing to the increasing Mach number along the jet centreline. Then the discharge phase starts. With $L_c > 1$ the attached shock stays in the first cell and, when it becomes detached, will be swept violently upstream. The shock stops after passing over the point of minimum density (L_m in figure 9) which has the highest Mach number and thus lowest stagnation pressure downstream of the shock. During the discharge phase, the shock position is controlled by stagnation pressure at the interface between two jets. The drop in p_r during the discharge phase reduces the interface stagnation pressure, resulting in a shift of the interface and shock wave downstream. Because of the continuing discharge, the shock is swept over the point of minimum density and therefore stagnation pressure rises above p_r . Thus the discharge phase is terminated. Rapid motion of the shock continues until it is stopped at the neck lip and the filling phase started again.

The main events controlling the oscillation can be described by the block diagram in figure 16(b). Filling of the resonator chamber ($u_z > 0$) occurs with stagnation pressure p_0 close or equal to $p_{0 \max}$, and raises the pressure p_r inside up to the level of $p_{0 \max}$. Increase in p_r suppresses the flow in the neck, finally causing the shock wave to jump upstream along ΔX and initiating the discharge phase ($u_z < 0$). During that phase the shock is moving slowly towards the point of minimum density in the jet cell and thus p_0 and p_r are tending to $p_{0 \min}$, but u_z to zero. In consequence the shock jumps to the neck lip and the filling phase can start again.

The oscillation process can also be shown as a transformation of the ambient supply

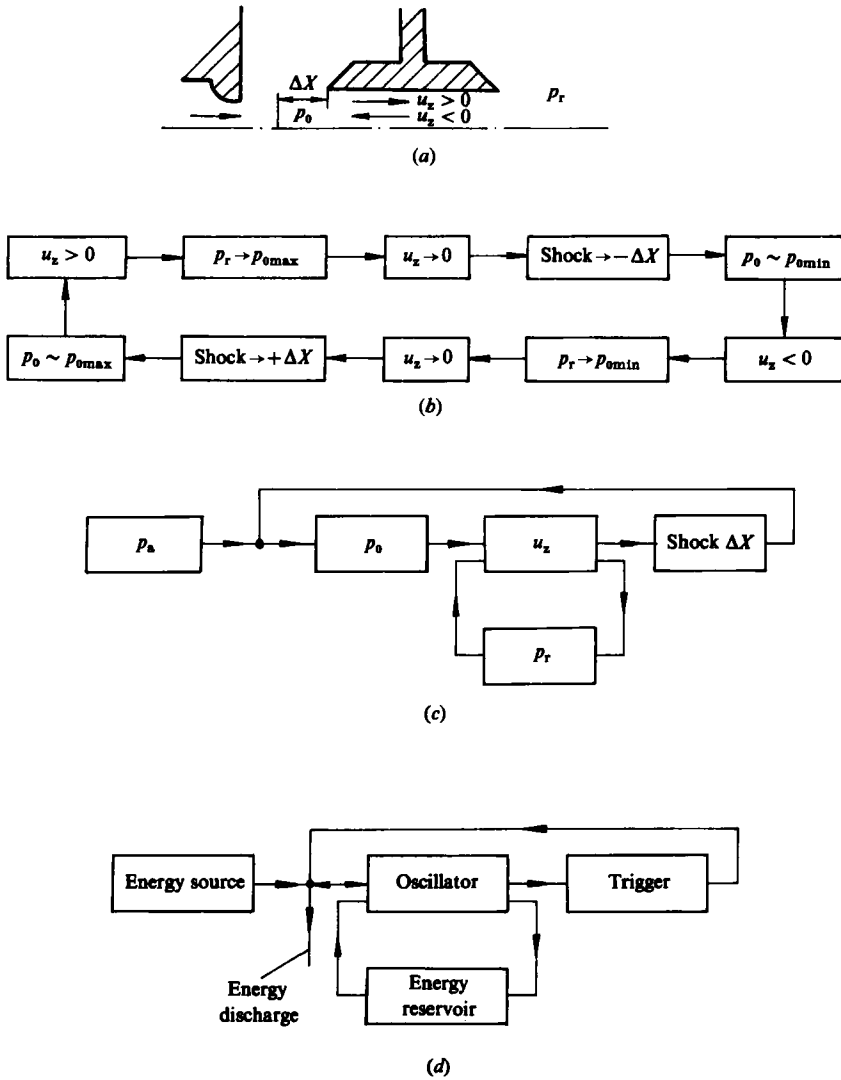


FIGURE 16. Block diagrams describing the oscillation.

pressure p_a to the jet stagnation pressure according to the shock-wave position, which in turn depends upon the air flow in the neck and the chamber pressure (figure 16c).

Applying a combination of basic schemes (Magnus 1961) of self-sustained oscillations, we may illustrate the phenomenon in a still more general form (figure 16d). A trigger controls energy flow from the source to the reservoir through the oscillator, and energy discharge outwards. The position of the trigger in turn depends upon the energy level in the reservoir and the energy flux in the oscillator. Such an oscillation possesses some properties of a relaxation-type oscillation.

The range of \bar{p} over which the regular and strong oscillation occurred depends to some extent on the ratio of spacing l to the cell length L_c . With decrease in \bar{p} the cell becomes longer and finally the detached shock related to $u_z = 0$ will be located upstream of the minimum density of the cell where it is stable. This determines the low- \bar{p} boundary of the oscillation and corresponds to a particular spacing l . When

\bar{p} , however, is low enough and strong shocks are permanent components of the cell structure, the detached shock has a much weaker influence on the stagnation pressure of the jet and the oscillation does not appear with any spacing l . The explanation of a much less distinct high- \bar{p} boundary is not so simple and explicit. Most probably also variation of p_0 with the shock displacement is not sufficient to support the strong oscillation. It becomes irregular and the amplitude is reduced considerably. By a proper adjustment to \bar{p} of the spacing l and the neck to nozzle-width ratio, the boundaries of \bar{p} associated with the oscillation can be somewhat extended.

Hartmann & Trolle's (1930) *modus operandi* of the air-jet pulsator is based on the mutual interaction of the stagnation pressure distributions along the jets from the nozzle and pulsator. He postulated that both distributions are of the same type. The cavity is filled until $p_r = p_{0 \max}$ is reached and then an unspecified disturbance starts the discharge phase which terminates with $p_r = p_{0 \min}$. The observations concerning p_r variation were absolutely correct and the discovery of instability zones, which are responsible for the oscillation, very important. Our photographs, however, indicate quite different structures of the jets emerging from the nozzle and from the neck. Hartmann's postulation is not necessary to explain the mechanism of the oscillation. Smith & Powell (1964) illuminated the role of the shock-wave displacement in the driving mechanism, which was omitted in Hartmann's considerations. They have also studied the oscillation with a Helmholtz resonator, but in their model identical shock waves appeared at both sides of the stagnation interface. Moreover this occurred in the second cell of the jet. What caused the starting of the shock displacement up- or downstream, still remained ambiguous. The authors of this paper believe that the dependence of the shock detachment on the flow in the neck indicated here yields a missing link in the chain of events, and the block diagram in figure 16 shows the mechanism of the oscillation somewhat better. It should be stressed that both of the above-mentioned investigations were related to the axisymmetric nozzle and cavity.

7. Concluding remarks

The experiments and theoretical considerations described in this paper were intended primarily to illuminate the mechanism of the basic self-sustained flow oscillation in the Hartmann generator with a Helmholtz resonator.

The study performed indicates that the oscillation mechanism is a relaxation type. It shows the generator investigated to be a bistable fluid flip-flop device. The instability of the shock wave along a jet cell is directly responsible for the oscillation. The oscillation occurs when a variation of the jet stagnation pressure with the shock-wave displacement and the entropy increase of the gas filling the resonator chamber are large enough. The variation in the stagnation pressure depends on the cell structure, resulting from a value of \bar{p} , and on the relative shock-wave positions controlled by the spacing l between the nozzle and the neck.

Regular oscillation was observed over $\bar{p} = 0.19\text{--}0.28$ and cell length/spacing ratio $L_c/l = 1.25\text{--}0.83$.

The pressure amplitude normalized by supply pressure was usually close to 0.1, but with $\bar{p} = 0.28$ and $L_c/l = 0.8$ reached a maximum level of 0.15. The oscillation frequency normalized with the natural frequency of a Helmholtz resonator varied between 0.75 and 1.06. No shock appeared between the stagnation interface and the neck lip during the discharge phase. Maximum pressure amplitudes at other positions in the plenum chamber were about 29% of the amplitude in the resonator chamber.

This implies a secondary dependence of the oscillations on the phenomena occurring further outside of the generator.

Compared to the oscillation frequencies reported above, it may be of interest that axisymmetric generators with a Helmholtz resonator produce very low-frequency oscillations. According to the experiments of Smith & Powell (1964) and W. M. Jungowski & G. B. Sobieraj (1980 unpublished results with Hartmann–Sprenger generators) the frequencies divided by f_H varied from 0.25 to 0.013 and 0.25 to 0.03 respectively, depending on the jet excess pressure and the spacing of the cavity and the nozzle.

The oscillation observed in the same test facility, but with a quarter-wave resonator, appeared very similar to that with a Helmholtz resonator. The normalized amplitude at the closed end, however, was about three times higher, reaching the value of 0.47. This was expected because the superiority of a quarter-wave resonator in the Hartmann–Sprenger generator is generally recognized.

The one-dimensional theory applied, despite the significant simplifying assumptions, yielded numerical results showing a good qualitative agreement with the experiment, except for the reversed frequency trend in the lower \bar{p} -range. The upper \bar{p} -boundary of the oscillation resulting from the computation performed fits reasonably well to the experimental one. The lower \bar{p} -boundary is about 16% higher than in the experiment. The computed pressure amplitudes were typically about 60% higher than the measured ones. The normalized frequency varied between 0.78 and 0.89.

The theoretical model made use of the following simplifications. The flow phenomena in the plenum chamber and the high-frequency oscillation in the neck were completely omitted as being of secondary importance. The entropy increase owing to the inlet and friction loss along the neck, and owing to the dissipation of kinetic energy in the resonator chamber was not included directly in the computation. It was, however, taken into account globally by introducing the parameter ϕ_r of entropy increase. This parameter must be large enough so that the frequency of the oscillation computed coincides with the monitored one. The crude estimation of a global entropy increase showed that the ϕ_r value introduced into the computation is realistic and physically justified. The theory made use of the experimental pressure distribution along the centreline of the jet, obtained with a steady flow. That way the cell distortion caused by a shear layer was taken into account.

A more rigorous theoretical treatment of flow in and around the generator, such as applying the Reynolds-averaged form of the compressible Navier–Stokes equation, would be very complex, time consuming, and require the involvement of a huge computer. That task seems to be more difficult than the computation of the self-sustained oscillation of a transonic flow past a two-dimensional aerofoil (Levy 1978 and Seegmiller, Marvin & Levy 1978) or of the oscillating flow in the open two-dimensional cavity (Hankey & Shang 1980). Moreover, it is doubtful whether such a procedure would lead to a much better understanding of the oscillation mechanism.

Because of a time limitation, the experimental efforts were concentrated on the main task, i.e. on the mechanism of the basic oscillation. Therefore, the investigation of local flow phenomena such as those at the neck lip or inside the neck was somewhat superficial. It seems that the flow separation and reattachment at the nozzle and at the neck, and the variation in the flow pattern in the region of the neck lip should be studied further in detail. The test facility secured in substance a fairly two-

dimensional flow. However, significant distortions of the cellular structure and the disappearance of the shock wave at certain instants could be partly a result of three-dimensional phenomena.

One of the authors (W.M.J.) gratefully acknowledges the fellowship provided by the Max-Planck-Society. Gratitude is extended to the Director of the Max-Planck-Institut für Strömungsforschung, Professor E.-A. Müller, for his friendly and helpful attitude. Both authors thank Dr G. E. A. Meier for his contributions during the course of this investigation. Thanks are also due to the referees for their valuable comments concerning this paper.

REFERENCES

- BOUCHER, H. & BRUN, E. 1958 Contribution à l'étude des ultrasons aériens: production et application. *Publication Scientifiques et Techniques du Ministère de L'Air* no. N.T. 79.
- BROCHER, E. & ARDISSONE, J.-P. 1983 Heating characteristics of a new type of Hartmann-Sprenger tube. *Intl J. Heat Fluid Flow* **4**, 97-102.
- BROCHER, E., MARESCA, A. & BOURNAY, M.-H. 1970 Fluid dynamics of the resonance tube. *J. Fluid Mech.* **43**, 369-384.
- BROCHER, E. & PINNA, G. 1980 Aeroacoustical phenomena in a horn excited by a Hartmann-Sprenger tube. *Acustica* **45**, 180-189.
- HANKEY, W. L. & SHANG, J. S. 1980 Analyses of pressure oscillations in an open cavity. *AIAA J.* **18**, 892-898.
- HARTMANN, J. & TROLLE, B. 1930 Modus operandi of the air-jet pulsator. *Dan Mat. Fys. Medd.* **10**, no. 4.
- IWAMOTO, J., KOBASHI, M., ARIGA, I. & WATANABE, I. 1976 On thermal effects of Hartmann-Sprenger tubes with various internal geometries. Presented at *Euromech 73, Oscillating Flows in Ducts, Aix-en Provence, 13-15 April*.
- JUNGOWSKI, W. M. 1978 Some self induced supersonic flow oscillations. *Prog. Aero. Sci.* **18**, 151-175.
- JUNGOWSKI, W. M. 1982 Self-sustained oscillations of gas flows as sources of discrete frequency noise. *Fortschritte der Akustik - FASE/DAGA '82*, pp. 79-91.
- JUNGOWSKI, W. M. & MEIER, G. E. A. 1984 Planar jets impinging on various obstacles and some modes of flow oscillation. *Mitteilungen aus dem Max-Planck-Institut für Strömungsforschung* Nr. 78.
- KAWAHASHI, M., BOBONE, R. & BROCHER, E. 1984 Oscillation modes in single-step Hartmann-Sprenger tubes. *J. Acoust. Soc. Am.* **75**, 780-784.
- KAWAHASHI, M., SASAKI, S., ANZAI, H. & SUZUKI, M. 1974 Unsteady, one-dimensional flow in resonance tube (with wall friction, heat transfer and interaction on a contact surface). *Bull JSME* **17**, 1555-1563.
- KAWAHASHI, M. & SUZUKI, M. 1974 Studies on resonance tube with a secondary resonator. *Bull. JSME* **17**, 595-602.
- KAWAHASHI, M. & SUZUKI, M. 1979 Generative mechanism of air column oscillations in a Hartmann-Sprenger tube excited by an air jet issuing from a convergent nozzle. *Z. Angew. Math. Phys.* **30**, 797-810.
- LEVY, L. L. 1978 Experimental and computational steady and unsteady transonic flows about a thick airfoil. *AIAA J.* **16**, 564-572.
- MAGNUS, K. 1961 *Schwingungen*. Stuttgart: B. G. Teubner.
- MØRCH, K. A. 1964 A theory for the mode of operation of the Hartmann air jet generator. *J. Fluid Mech.* **20**, 141-159.
- PRZIREMBEL, C. E. G. & FLETCHER, L. S. 1978 Aerothermodynamic characteristics of a resonance tube driven by a subsonic jet. *AIAA J.* **16**, 184-186.
- PRZIREMBEL, C. E. G., FLETCHER, L. S. & WOLF, D. E. 1977 Thermodynamic characteristics of a blunt two-dimensional resonance tube. *AIAA J.* **15**, 905-906.

- ROCKWELL, D. 1983 Oscillations of impinging shear layers. *AIAA J.* **21**, 645–664.
- ROCKWELL, D. & NAUDASCHER, E. 1979 Self-sustained oscillations of impinging free shear layers. *Ann. Rev. Fluid Mech.* **11**, 67–94.
- ROZENBERG, L. D. (ed.) 1969 *Sources of High-Intensity Ultrasound*, pp. 1–162. Plenum.
- SAROHIA, V. & BACK, L. H. 1979 Experimental investigation of flow and heating in a resonance tube. *J. Fluid Mech.* **94**, 649–672.
- SEEGMILLER, H. L., MARVIN, J. G. LEVY, L. L. 1976 Steady and unsteady transonic flow. *AIAA J.* **16**, 1262–1270.
- SMITH, T. J. B. & POWELL, A. 1964 Experiments concerning the Hartmann whistle. *Dept. of Engin., Univ. of Calif., Rep.* 64–42.
- SPRENGER, H. 1954 Über thermische Effekte in Resonanzrohren. *Mitteilungen aus dem Institut für Aerodynamik an der E.T.H. Zürich, Nr.* 21, pp. 18–35.
- STASICKI, B. & MEIER, G. E. A. 1976 Konstanttemperatur-Anemometersystem ASM 1. *Max-Planck-Institut für Strömungsforschung, Göttingen, Ber.* 103.
- THOMPSON, P. A. 1964 Jet-driven resonance tube. *AIAA J.* **2**, 1230–1233.
- VREBALOVICH, T. 1962 Resonance tubes in a supersonic flow field. *Jet. Prop. Lab., Cal. Inst. of Techn., Pasadena, T.R. no.* 32–37d.